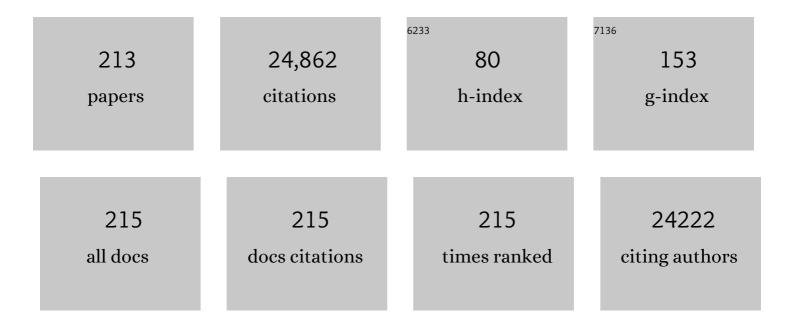
Cheng Wang

List of Publications by Year in descending order

Source: https://exaly.com/author-pdf/1049359/publications.pdf Version: 2024-02-01



#	Article	IF	CITATIONS
1	Importance of Highâ€Electron Mobility in Polymer Acceptors for Efficient Allâ€Polymer Solar Cells: Combined Engineering of Backbone Building Unit and Regioregularity. Advanced Functional Materials, 2022, 32, 2108508.	7.8	41
2	Decoupling Complex Multiâ€Lengthâ€Scale Morphology in Nonâ€Fullerene Photovoltaics with Nitrogen Kâ€Edge Resonant Soft Xâ€ray Scattering. Advanced Materials, 2022, 34, e2107316.	11.1	16
3	Cation-Gated Ion Transport at Nanometer Scale for Tunable Power Generation. Journal of Physical Chemistry Letters, 2022, 13, 2625-2631.	2.1	3
4	High-brightness all-polymer stretchable LED with charge-trapping dilution. Nature, 2022, 603, 624-630.	13.7	170
5	Twoâ€Photon 3D Printing in Metal–Organic Framework Single Crystals. Small, 2022, 18, e2200514.	5.2	15
6	Controlling spontaneous chirality in achiral materials: liquid crystal oligomers and the heliconical twist-bend nematic phase. Chemical Communications, 2022, 58, 5285-5288.	2.2	17
7	Enabling alcohol as a hydrogen carrier using metal–organic framework-stabilized Ir–Sc bifunctional catalytic sites. Chemical Communications, 2022, 58, 5857-5860.	2.2	2
8	Magnetic 3d–4f Chiral Clusters Showing Multimetal Site Magneto-Chiral Dichroism. Journal of the American Chemical Society, 2022, 144, 8837-8847.	6.6	28
9	<i>Operando</i> Resonant Soft X-ray Scattering Studies of Chemical Environment and Interparticle Dynamics of Cu Nanocatalysts for CO ₂ Electroreduction. Journal of the American Chemical Society, 2022, 144, 8927-8931.	6.6	18
10	Two-dimensional metal–organic layers constructed from Hf ₆ /Hf ₁₂ -oxo clusters and a trigonal pyramidal phosphine oxide ligand. Dalton Transactions, 2022, 51, 11236-11240.	1.6	4
11	Thio linkage between CdS quantum dots and UiO-66-type MOFs as an effective transfer bridge of charge carriers boosting visible-light-driven photocatalytic hydrogen production. Journal of Colloid and Interface Science, 2021, 581, 1-10.	5.0	73
12	Efficient, Thermally Stable, and Mechanically Robust Allâ€Polymer Solar Cells Consisting of the Same Benzodithiophene Unitâ€Based Polymer Acceptor and Donor with High Molecular Compatibility. Advanced Energy Materials, 2021, 11, 2003367.	10.2	122
13	Two-photon induced polymerization in a porous polymer film to create multi-layer structures. Chemical Communications, 2021, 57, 4516-4519.	2.2	5
14	Soluble lanthanide-transition-metal clusters Ln36Co12 as effective molecular electrocatalysts for water oxidation. Chemical Communications, 2021, 57, 3611-3614.	2.2	13
15	Metal–organic frameworks embedded in a liposome facilitate overall photocatalytic water splitting. Nature Chemistry, 2021, 13, 358-366.	6.6	168
16	Metal–Organic Layers with an Enhanced Two-Photon Absorption Cross-Section and Up-Converted Emission. Chemistry of Materials, 2021, 33, 1618-1624.	3.2	8
17	Bifunctional Metal–Organic Layer with Organic Dyes and Iron Centers for Synergistic Photoredox Catalysis. Journal of the American Chemical Society, 2021, 143, 3075-3080.	6.6	60
18	Excited State Energy Transfer in Metalâ€Organic Frameworks. Advanced Materials, 2021, 33, e2005819.	11.1	34

#	Article	IF	CITATIONS
19	Molecular Origin of Strainâ€Induced Chain Alignment in PDPPâ€Based Semiconducting Polymeric Thin Films. Advanced Functional Materials, 2021, 31, 2100161.	7.8	38
20	Machine-Learning-Guided Discovery and Optimization of Additives in Preparing Cu Catalysts for CO ₂ Reduction. Journal of the American Chemical Society, 2021, 143, 5755-5762.	6.6	81
21	Label-free characterization of organic nanocarriers reveals persistent single molecule cores for hydrocarbon sequestration. Nature Communications, 2021, 12, 3123.	5.8	9
22	Fullerene–non-fullerene hybrid acceptors for enhanced light absorption and electrical properties in organic solar cells. Materials Today Energy, 2021, 20, 100651.	2.5	7
23	Probing morphology and chemistry in complex soft materials with in situ resonant soft x-ray scattering. Journal of Physics Condensed Matter, 2021, 33, 313001.	0.7	5
24	Neighboring Zn–Zr Sites in a Metal–Organic Framework for CO ₂ Hydrogenation. Journal of the American Chemical Society, 2021, 143, 8829-8837.	6.6	82
25	Diversifying Composition Leads to Hierarchical Composites with Design Flexibility and Structural Fidelity. ACS Nano, 2021, 15, 14095-14104.	7.3	9
26	Photonic Bandgap in Achiral Liquid Crystals—A Twist on a Twist. Advanced Materials, 2021, 33, e2103288.	11.1	18
27	Bifunctional Metal–Organic Layers for Tandem Catalytic Transformations Using Molecular Oxygen and Carbon Dioxide. Journal of the American Chemical Society, 2021, 143, 16718-16724.	6.6	28
28	Preparation of hollow metal–organic frameworks <i>via</i> epitaxial protection and selective etching. Faraday Discussions, 2021, 231, 181-193.	1.6	3
29	Sulfate-functionalized metal–organic frameworks supporting Pd nanoparticles for the hydrogenolysis of glycerol to 1,2-propanediol. New Journal of Chemistry, 2021, 45, 21263-21269.	1.4	8
30	Thickness Dependence of Proton-Exchange-Membrane Properties. Journal of the Electrochemical Society, 2021, 168, 104517.	1.3	10
31	Donor–Acceptor Alternating Copolymer Compatibilizers for Thermally Stable, Mechanically Robust, and High-Performance Organic Solar Cells. ACS Nano, 2021, 15, 19970-19980.	7.3	38
32	ZnO Supported on a Zr-Based Metal–Organic Framework for Selective CO ₂ Hydrogenation to Methanol. ACS Applied Energy Materials, 2021, 4, 13567-13574.	2.5	12
33	Photoactivation of Cu Centers in Metal–Organic Frameworks for Selective CO ₂ Conversion to Ethanol. Journal of the American Chemical Society, 2020, 142, 75-79.	6.6	95
34	Unraveling the Crystallization Kinetics of 2D Perovskites with Sandwichâ€īype Structure for Highâ€Performance Photovoltaics. Advanced Materials, 2020, 32, e2002784.	11.1	52
35	Improving Efficiency and Stability of Perovskite Solar Cells Enabled by A Near-Infrared-Absorbing Moisture Barrier. Joule, 2020, 4, 1575-1593.	11.7	88
36	Natural optical activity as the origin of the large chiroptical properties in π-conjugated polymer thin films. Nature Communications, 2020, 11, 6137.	5.8	73

#	Article	IF	CITATIONS
37	Blue Energy Conversion from Holey-Graphene-like Membranes with a High Density of Subnanometer Pores. Nano Letters, 2020, 20, 8634-8639.	4.5	42
38	New Insights into Water Treatment Materials with Chemically Sensitive Soft and Tender X-rays. Synchrotron Radiation News, 2020, 33, 17-23.	0.2	5
39	Metal–Organic Layers for Electrocatalysis and Photocatalysis. ACS Central Science, 2020, 6, 2149-2158.	5.3	54
40	Bimolecular crystal instability and morphology of bulk heterojunction blends in organic and perovskite solar cells. Journal of Materials Chemistry C, 2020, 8, 11695-11703.	2.7	1
41	Manipulating Film Morphology of Allâ€Polymer Solar Cells by Incorporating Polymer Compatibilizer. Solar Rrl, 2020, 4, 2000148.	3.1	16
42	Photoresponsive 2D polymeric Langmuir–Blodgett films of 2,3,6,7,10,11-hexaiminotriphenylene. New Journal of Chemistry, 2020, 44, 5656-5660.	1.4	9
43	Genetically targeted chemical assembly of functional materials in living cells, tissues, and animals. Science, 2020, 367, 1372-1376.	6.0	132
44	Nanoscale Metal–Organic Frameworks and Metal–Organic Layers with Two-Photon-Excited Fluorescence. Inorganic Chemistry, 2020, 59, 4181-4185.	1.9	13
45	Highly Dispersed Ni Catalyst on Metal–Organic Framework-Derived Porous Hydrous Zirconia for CO ₂ Methanation. ACS Applied Materials & Interfaces, 2020, 12, 17436-17442.	4.0	64
46	Metal–Organic Framework with Dual Active Sites in Engineered Mesopores for Bioinspired Synergistic Catalysis. Journal of the American Chemical Society, 2020, 142, 8602-8607.	6.6	53
47	Chemical and Morphological Origins of Improved Ion Conductivity in Perfluoro Ionene Chain Extended Ionomers. Journal of the American Chemical Society, 2019, 141, 13547-13561.	6.6	34
48	Sulfur-linked cyanobiphenyl-based liquid crystal dimers and the twist-bend nematic phase. Liquid Crystals, 2019, 46, 1595-1609.	0.9	85
49	Energy transfer on a two-dimensional antenna enhances the photocatalytic activity of CO2 reduction by metal–organic layers. Chemical Communications, 2019, 55, 9657-9660.	2.2	23
50	Titanium Hydroxide Secondary Building Units in Metal–Organic Frameworks Catalyze Hydrogen Evolution under Visible Light. Journal of the American Chemical Society, 2019, 141, 12219-12223.	6.6	86
51	Cooperative copper centres in a metal–organic framework for selective conversion of CO2 to ethanol. Nature Catalysis, 2019, 2, 709-717.	16.1	256
52	Cooperative Stabilization of the [Pyridinium-CO ₂ -Co] Adduct on a Metal–Organic Layer Enhances Electrocatalytic CO ₂ Reduction. Journal of the American Chemical Society, 2019, 141, 17875-17883.	6.6	108
53	Processing-Friendly Slot-Die-Cast Nonfullerene Organic Solar Cells with Optimized Morphology. ACS Applied Materials & Interfaces, 2019, 11, 42392-42402.	4.0	29
54	Strongly Lewis Acidic Metal–Organic Frameworks for Continuous Flow Catalysis. Journal of the American Chemical Society, 2019, 141, 14878-14888.	6.6	118

#	Article	IF	CITATIONS
55	Photoacid-Modified Nafion Membrane Morphology Determined by Resonant X-ray Scattering and Spectroscopy. ACS Macro Letters, 2019, 8, 1353-1359.	2.3	7
56	Cobalt-bridged secondary building units in a titanium metal–organic framework catalyze cascade reduction of N-heteroarenes. Chemical Science, 2019, 10, 2193-2198.	3.7	40
57	Metal–Organic Framework Stabilizes a Low-Coordinate Iridium Complex for Catalytic Methane Borylation. Journal of the American Chemical Society, 2019, 141, 11196-11203.	6.6	65
58	Twoâ€Dimensional Metalâ€Organic Layers for Electrochemical Acceptorless Dehydrogenation of Nâ€Heterocycles. Chemistry - an Asian Journal, 2019, 14, 3557-3560.	1.7	19
59	Multi-level chirality in liquid crystals formed by achiral molecules. Nature Communications, 2019, 10, 1922.	5.8	103
60	Aluminum Hydroxide Secondary Building Units in a Metal–Organic Framework Support Earth-Abundant Metal Catalysts for Broad-Scope Organic Transformations. ACS Catalysis, 2019, 9, 3327-3337.	5.5	46
61	In Situ Structure Characterization in Slotâ€Dieâ€Printed Allâ€Polymer Solar Cells with Efficiency Over 9%. Solar Rrl, 2019, 3, 1900032.	3.1	20
62	Aluminum oxide free-standing thin films to enable nitrogen edge soft x-ray scattering. MRS Communications, 2019, 9, 224-228.	0.8	6
63	Metal–Organic Frameworks in Solid–Gas Phase Catalysis. ACS Catalysis, 2019, 9, 130-146.	5.5	229
64	Metal–Organic Framework Nodes Support Single-Site Nickel(II) Hydride Catalysts for the Hydrogenolysis of Aryl Ethers. ACS Catalysis, 2019, 9, 1578-1583.	5.5	61
65	Surpassing 10% Efficiency Benchmark for Nonfullerene Organic Solar Cells by Scalable Coating in Air from Single Nonhalogenated Solvent. Advanced Materials, 2018, 30, 1705485.	11.1	150
66	Metal–organic layers stabilize earth-abundant metal–terpyridine diradical complexes for catalytic C–H activation. Chemical Science, 2018, 9, 143-151.	3.7	75
67	Understanding the Impact of Oligomeric Polystyrene Side Chain Arrangement on the Allâ€Polymer Solar Cell Performance. Advanced Energy Materials, 2018, 8, 1701552.	10.2	21
68	A Dynamically Stabilized Singleâ€Nickel Electrocatalyst for Selective Reduction of Oxygen to Hydrogen Peroxide. Chemistry - A European Journal, 2018, 24, 17011-17018.	1.7	13
69	Frontispiece: A Dynamically Stabilized Singleâ€Nickel Electrocatalyst for Selective Reduction of Oxygen to Hydrogen Peroxide. Chemistry - A European Journal, 2018, 24, .	1.7	0
70	Simulating Powder X-ray Diffraction Patterns of Two-Dimensional Materials. Inorganic Chemistry, 2018, 57, 15123-15132.	1.9	36
71	Two-Dimensional Metal–Organic Layers on Carbon Nanotubes to Overcome Conductivity Constraint in Electrocatalysis. ACS Applied Materials & Interfaces, 2018, 10, 36290-36296.	4.0	51
72	Random Copolymers Allow Control of Crystallization and Microphase Separation in Fully Conjugated Block Copolymers. Macromolecules, 2018, 51, 8844-8852.	2.2	15

#	Article	IF	CITATIONS
73	Photosensitizing Metal–Organic Layers for Efficient Sunlight-Driven Carbon Dioxide Reduction. Journal of the American Chemical Society, 2018, 140, 12369-12373.	6.6	164
74	Resonant Soft X-Ray Scattering Provides Protein Structure with Chemical Specificity. Structure, 2018, 26, 1513-1521.e3.	1.6	10
75	Synthetic Strategies for Constructing Twoâ€Dimensional Metalâ€Organic Layers (MOLs): A Tutorial Review. Chinese Journal of Chemistry, 2018, 36, 754-764.	2.6	61
76	Resonant soft X-ray scattering reveals cellulose microfibril spacing in plant primary cell walls. Scientific Reports, 2018, 8, 12449.	1.6	26
77	Photo-generated dinuclear {Eu(II)}2 active sites for selective CO2 reduction in a photosensitizing metal-organic framework. Nature Communications, 2018, 9, 3353.	5.8	195
78	Resonant soft x-ray scattering unravels the hierarchical morphology of nanostructured bulk heterojunction photovoltaic thin films. Physical Review Materials, 2018, 2, .	0.9	4
79	Confinement of Ultrasmall Cu/ZnO _{<i>x</i>} Nanoparticles in Metal–Organic Frameworks for Selective Methanol Synthesis from Catalytic Hydrogenation of CO ₂ . Journal of the American Chemical Society, 2017, 139, 3834-3840.	6.6	463
80	Rollâ€ŧoâ€Roll Printed Largeâ€Area Allâ€Polymer Solar Cells with 5% Efficiency Based on a Low Crystallinity Conjugated Polymer Blend. Advanced Energy Materials, 2017, 7, 1602742.	10.2	214
81	Quantifying the Hierarchical Order in Self-Aligned Carbon Nanotubes from Atomic to Micrometer Scale. ACS Nano, 2017, 11, 5405-5416.	7.3	39
82	Twoâ€Dimensional Metalâ€Organic Layers as a Bright and Processable Phosphor for Fast Whiteâ€Light Communication. Chemistry - A European Journal, 2017, 23, 8390-8394.	1.7	47
83	Exciton Migration and Amplified Quenching on Two-Dimensional Metal–Organic Layers. Journal of the American Chemical Society, 2017, 139, 7020-7029.	6.6	134
84	Surface Modification of Twoâ€Dimensional Metal–Organic Layers Creates Biomimetic Catalytic Microenvironments for Selective Oxidation. Angewandte Chemie - International Edition, 2017, 56, 9704-9709.	7.2	155
85	In situ dynamic observations of perovskite crystallisation and microstructure evolution intermediated from [Pbl6]4â^² cage nanoparticles. Nature Communications, 2017, 8, 15688.	5.8	191
86	Electron Crystallography Reveals Atomic Structures of Metal–Organic Nanoplates with M ₁₂ (μ ₃ -O) ₈ (μ ₃ -OH) ₈ -OH) <td>∙H)<r⊾øb>6∙</td> <td></td>	∙H)< r⊾ø b>6∙	
87	Surface Modification of Twoâ€Dimensional Metal–Organic Layers Creates Biomimetic Catalytic Microenvironments for Selective Oxidation. Angewandte Chemie, 2017, 129, 9836-9841.	1.6	38
88	Pyrolysis of metal–organic frameworks to hierarchical porous Cu/Zn-nanoparticle@carbon materials for efficient CO ₂ hydrogenation. Materials Chemistry Frontiers, 2017, 1, 2405-2409.	3.2	54
89	Importance of 2D Conjugated Side Chains of Benzodithiophene-Based Polymers in Controlling Polymer Packing, Interfacial Ordering, and Composition Variations of All-Polymer Solar Cells. Chemistry of Materials, 2017, 29, 9407-9415.	3.2	67
90	Structure of nanoscale-pitch helical phases: blue phase and twist-bend nematic phase resolved by resonant soft X-ray scattering. Soft Matter, 2017, 13, 6694-6699.	1.2	70

#	Article	IF	CITATIONS
91	Warm-White-Light-Emitting Diode Based on a Dye-Loaded Metal–Organic Framework for Fast White-Light Communication. ACS Applied Materials & Interfaces, 2017, 9, 35253-35259.	4.0	99
92	Through-space Förster-type energy transfer in isostructural zirconium and hafnium-based metal–organic layers. Chemical Communications, 2017, 53, 9356-9359.	2.2	21
93	Frontispiece: Surface Modification of Twoâ€Dimensional Metal–Organic Layers Creates Biomimetic Catalytic Microenvironments for Selective Oxidation. Angewandte Chemie - International Edition, 2017, 56, .	7.2	0
94	Frontispiz: Surface Modification of Twoâ€Dimensional Metal–Organic Layers Creates Biomimetic Catalytic Microenvironments for Selective Oxidation. Angewandte Chemie, 2017, 129, .	1.6	0
95	Molecular Iridium Complexes in Metal–Organic Frameworks Catalyze CO ₂ Hydrogenation via Concerted Proton and Hydride Transfer. Journal of the American Chemical Society, 2017, 139, 17747-17750.	6.6	135
96	Electrocatalytic reduction of CO ₂ to CO with 100% faradaic efficiency by using pyrolyzed zeolitic imidazolate frameworks supported on carbon nanotube networks. Journal of Materials Chemistry A, 2017, 5, 24867-24873.	5.2	78
97	Networking Pyrolyzed Zeolitic Imidazolate Frameworks by Carbon Nanotubes Improves Conductivity and Enhances Oxygenâ€Reduction Performance in Polymerâ€Electrolyteâ€Membrane Fuel Cells. Advanced Materials, 2017, 29, 1604556.	11.1	131
98	A multifunctional biphasic water splitting catalyst tailored for integration with high-performance semiconductor photoanodes. Nature Materials, 2017, 16, 335-341.	13.3	217
99	A Rheniumâ€Functionalized Metal–Organic Framework as a Singleâ€Site Catalyst for Photochemical Reduction of Carbon Dioxide. European Journal of Inorganic Chemistry, 2016, 2016, 4358-4362.	1.0	70
100	Combining theory and experiment for X-ray absorption spectroscopy and resonant X-ray scattering characterization of polymers. Polymer, 2016, 99, 782-796.	1.8	17
101	Postsynthetic Modification of Metalâ€Organic Frameworks through Click Chemistry. Chinese Journal of Chemistry, 2016, 34, 186-190.	2.6	33
102	Self‣upporting Metal–Organic Layers as Single‣ite Solid Catalysts. Angewandte Chemie - International Edition, 2016, 55, 4962-4966.	7.2	303
103	Correlation between Phase-Separated Domain Sizes of Active Layer and Photovoltaic Performances in All-Polymer Solar Cells. Macromolecules, 2016, 49, 5051-5058.	2.2	93
104	A 2D porous porphyrin-based covalent organic framework for sulfur storage in lithium–sulfur batteries. Journal of Materials Chemistry A, 2016, 4, 7416-7421.	5.2	267
105	Following the Morphology Formation In Situ in Printed Active Layers for Organic Solar Cells. Advanced Energy Materials, 2016, 6, 1501580.	10.2	82
106	Innenrücktitelbild: Self-Supporting Metal-Organic Layers as Single-Site Solid Catalysts (Angew. Chem.) Tj ETQq0) 0 0 rgBT 1.0 rgBT	/Qverlock 1
107	Resonant soft X-ray scattering for polymer materials. European Polymer Journal, 2016, 81, 555-568.	2.6	79

Pyrolysis of Metal–Organic Frameworks to Fe₃O₄@Fe₅C₂ Core–Shell Nanoparticles for Fischer–Tropsch Synthesis. ACS Catalysis, 2016, 6, 3610-3618. 108 5.5 138

#	Article	IF	CITATIONS
109	Revisiting the interpretation of casein micelle SAXS data. Soft Matter, 2016, 12, 6937-6953.	1.2	78
110	Comparison of the Morphology Development of Polymer–Fullerene and Polymer–Polymer Solar Cells during Solution‧hearing Blade Coating. Advanced Energy Materials, 2016, 6, 1601225.	10.2	79
111	Controlling Energy Levels and Blend Morphology for All-Polymer Solar Cells via Fluorination of a Naphthalene Diimide-Based Copolymer Acceptor. Macromolecules, 2016, 49, 6374-6383.	2.2	66
112	Side Chain Optimization of Naphthalenediimide–Bithiopheneâ€Based Polymers to Enhance the Electron Mobility and the Performance in Allâ€Polymer Solar Cells. Advanced Functional Materials, 2016, 26, 1543-1553.	7.8	155
113	Resonant Carbon <mml:math <br="" xmlns:mml="http://www.w3.org/1998/Math/MathML">display="inline"><mml:mrow><mml:mi>K</mml:mi></mml:mrow></mml:math> -Edge Soft X-Ray Scattering from Lattice-Free Heliconical Molecular Ordering: Soft Dilative Elasticity of the Twist-Bend Liquid Crystal Phase. Physical Review Letters. 2016. 116. 147803.	2.9	157
114	Metal–Organic Frameworks Stabilize Mono(phosphine)–Metal Complexes for Broad-Scope Catalytic Reactions. Journal of the American Chemical Society, 2016, 138, 9783-9786.	6.6	111
115	Highâ€Efficiency Nonfullerene Polymer Solar Cells with Medium Bandgap Polymer Donor and Narrow Bandgap Organic Semiconductor Acceptor. Advanced Materials, 2016, 28, 8288-8295.	11.1	247
116	Bacteriophytochrome Photoisomerization Proceeds Homogeneously Despite Heterogeneity in Ground State. Biophysical Journal, 2016, 111, 2125-2134.	0.2	21
117	Reprint of: Combining theory and experiment for X-ray absorption spectroscopy and resonant X-ray scattering characterization of polymers. Polymer, 2016, 105, 342-356.	1.8	8
118	Mechanized azobenzene-functionalized zirconium metal-organic framework for on-command cargo release. Science Advances, 2016, 2, e1600480.	4.7	188
119	Fabrication of bilayer tetrathiafulvalene integrated surface covalent organic frameworks. Physical Chemistry Chemical Physics, 2016, 18, 17356-17359.	1.3	19
120	Two-dimensional porphyrin- and phthalocyanine-based covalent organic frameworks. Chinese Chemical Letters, 2016, 27, 1376-1382.	4.8	64
121	Self‣upporting Metal–Organic Layers as Single‣ite Solid Catalysts. Angewandte Chemie, 2016, 128, 5046-5050.	1.6	61
122	Polydimethylsiloxane/covalent triazine frameworks coated stir bar sorptive extraction coupled with high performance liquid chromatography-ultraviolet detection for the determination of phenols in environmental water samples. Journal of Chromatography A, 2016, 1441, 8-15.	1.8	93
123	Förster Energy Transport in Metal–Organic Frameworks Is Beyond Step-by-Step Hopping. Journal of the American Chemical Society, 2016, 138, 5308-5315.	6.6	131
124	Sulfur-doping achieves efficient oxygen reduction in pyrolyzed zeolitic imidazolate frameworks. Journal of Materials Chemistry A, 2016, 4, 4457-4463.	5.2	65
125	A Pyrene-Based, Fluorescent Three-Dimensional Covalent Organic Framework. Journal of the American Chemical Society, 2016, 138, 3302-3305.	6.6	628
126	Communication: Coherences observed <i>in vivo</i> in photosynthetic bacteria using two-dimensional electronic spectroscopy. Journal of Chemical Physics, 2015, 143, 101101.	1.2	26

#	Article	IF	CITATIONS
127	Probing and Controlling Liquid Crystal Helical Nanofilaments. Nano Letters, 2015, 15, 3420-3424.	4.5	42
128	Pore surface engineering in a zirconium metal–organic framework via thiol-ene reaction. Journal of Solid State Chemistry, 2015, 223, 79-83.	1.4	20
129	Determining the Role of Polymer Molecular Weight for High-Performance All-Polymer Solar Cells: Its Effect on Polymer Aggregation and Phase Separation. Journal of the American Chemical Society, 2015, 137, 2359-2365.	6.6	347
130	Photosensitizing Metal–Organic Framework Enabling Visible-Light-Driven Proton Reduction by a Wells–Dawson-Type Polyoxometalate. Journal of the American Chemical Society, 2015, 137, 3197-3200.	6.6	374
131	Tackling poison and leach: catalysis by dangling thiol–palladium functions within a porous metal–organic solid. Chemical Communications, 2015, 51, 6917-6920.	2.2	59
132	Highâ€Performance Allâ€Polymer Solar Cells Via Sideâ€Chain Engineering of the Polymer Acceptor: The Importance of the Polymer Packing Structure and the Nanoscale Blend Morphology. Advanced Materials, 2015, 27, 2466-2471.	11.1	279
133	Towards quantification of vibronic coupling in photosynthetic antenna complexes. Journal of Chemical Physics, 2015, 142, 212446.	1.2	25
134	Highly Active Hydrogen Evolution Electrodes via Co-Deposition of Platinum and Polyoxometalates. ACS Applied Materials & Interfaces, 2015, 7, 11648-11653.	4.0	46
135	Heterogeneity of functional groups in a metal–organic framework displays magic number ratios. Proceedings of the National Academy of Sciences of the United States of America, 2015, 112, 5591-5596.	3.3	36
136	Postsynthetic Modification of an Alkyne-Tagged Zirconium Metal–Organic Framework via a "Click― Reaction. Inorganic Chemistry, 2015, 54, 5139-5141.	1.9	51
137	Solving the mystery of the internal structure of casein micelles. Soft Matter, 2015, 11, 2723-2725.	1.2	68
138	Pre-concentration and energy transfer enable the efficient luminescence sensing of transition metal ions by metal–organic frameworks. Chemical Communications, 2015, 51, 16996-16999.	2.2	55
139	Flow-enhanced solution printing of all-polymer solar cells. Nature Communications, 2015, 6, 7955.	5.8	221
140	Substrate Orientation Effect in the On-Surface Synthesis of Tetrathiafulvalene-Integrated Single-Layer Covalent Organic Frameworks. Langmuir, 2015, 31, 11755-11759.	1.6	36
141	Flexible, highly efficient all-polymer solar cells. Nature Communications, 2015, 6, 8547.	5.8	740
142	Reversible Tuning Hydroquinone/Quinone Reaction in Metal–Organic Framework: Immobilized Molecular Switches in Solid State. Chemistry of Materials, 2015, 27, 6426-6431.	3.2	72
143	Simultaneous spin-coating and solvent annealing: manipulating the active layer morphology to a power conversion efficiency of 9.6% in polymer solar cells. Materials Horizons, 2015, 2, 592-597.	6.4	32
144	Controllable Synthesis of Covalent Porphyrinic Cages with Varying Sizes via Template-Directed Imine Condensation Reactions. Journal of Organic Chemistry, 2015, 80, 9360-9364.	1.7	16

#	Article	IF	CITATIONS
145	Fast Printing and In Situ Morphology Observation of Organic Photovoltaics Using Slotâ€Die Coating. Advanced Materials, 2015, 27, 886-891.	11.1	117
146	Targeted synthesis of a large triazine-based [4+6] organic molecular cage: structure, porosity and gas separation. Chemical Communications, 2015, 51, 1976-1979.	2.2	85
147	Gadolinium nicotinate clusters as potential MRI contrast agents. RSC Advances, 2015, 5, 2914-2919.	1.7	4
148	A Mechanistic Understanding of Processing Additiveâ€Induced Efficiency Enhancement in Bulk Heterojunction Organic Solar Cells. Advanced Materials, 2014, 26, 300-305.	11.1	145
149	Understanding the Morphology of PTB7:PCBM Blends in Organic Photovoltaics. Advanced Energy Materials, 2014, 4, 1301377.	10.2	203
150	The Effects of Electron-Donating Substituents on [lr(bpy)Cp*Cl]+: Water Oxidation versus Ligand Oxidative Modifications. European Journal of Inorganic Chemistry, 2014, 2014, 698-707.	1.0	27
151	A Biomimetic Copper Water Oxidation Catalyst with Low Overpotential. Journal of the American Chemical Society, 2014, 136, 273-281.	6.6	339
152	Functional Metal–Organic Frameworks via Ligand Doping: Influences of Ligand Charge and Steric Demand. Inorganic Chemistry, 2014, 53, 1331-1338.	1.9	32
153	A Tetrathiafulvaleneâ€Based Electroactive Covalent Organic Framework. Chemistry - A European Journal, 2014, 20, 14614-14618.	1.7	143
154	Highly-efficient synthesis of covalent porphyrinic cages via DABCO-templated imine condensation reactions. Chemical Communications, 2014, 50, 11162.	2.2	27
155	A hybrid polyoxometalate–organic molecular catalyst for visible light driven water oxidation. Chemical Communications, 2014, 50, 11591-11594.	2.2	26
156	Guided crystallization of P3HT in ternary blend solar cell based on P3HT:PCPDTBT:PCBM. Energy and Environmental Science, 2014, 7, 3782-3790.	15.6	60
157	Mechanical Bonds and Topological Effects in Radical Dimer Stabilization. Journal of the American Chemical Society, 2014, 136, 11011-11026.	6.6	47
158	Synergistic Assembly of Heavy Metal Clusters and Luminescent Organic Bridging Ligands in Metal–Organic Frameworks for Highly Efficient X-ray Scintillation. Journal of the American Chemical Society, 2014, 136, 6171-6174.	6.6	198
159	Covalent-organic frameworks: potential host materials for sulfur impregnation in lithium–sulfur batteries. Journal of Materials Chemistry A, 2014, 2, 8854-8858.	5.2	229
160	Porous Organic Molecular Cages: from Preparation to Applications. Current Organic Chemistry, 2014, 18, 1965-1972.	0.9	15
161	Metal–Organic Frameworks as A Tunable Platform for Designing Functional Molecular Materials. Journal of the American Chemical Society, 2013, 135, 13222-13234.	6.6	801
162	Relating Chemical Structure to Device Performance via Morphology Control in Diketopyrrolopyrrole-Based Low Band Gap Polymers. Journal of the American Chemical Society, 2013, 135, 19248-19259.	6.6	121

#	Article	IF	CITATIONS
163	Signatures of Multiphase Formation in the Active Layer of Organic Solar Cells from Resonant Soft X-ray Scattering. ACS Macro Letters, 2013, 2, 185-189.	2.3	37
164	Threeâ€Dimensional Architectures Incorporating Stereoregular Donor–Acceptor Stacks. Chemistry - A European Journal, 2013, 19, 8457-8465.	1.7	28
165	Effect of Nonsolvent Exposure on Morphology of Mesoporous Semicrystalline Block Copolymer Films. Macromolecules, 2013, 46, 4411-4417.	2.2	12
166	Morphology and Optical Properties of P3HT:MEH-CN-PPV Blend Films. Macromolecules, 2013, 46, 4491-4501.	2.2	47
167	Accurate and Facile Determination of the Index of Refraction of Organic Thin Films Near the Carbon <mml:math <br="" xmlns:mml="http://www.w3.org/1998/Math/MathML">display="inline"><mml:mn>1</mml:mn><mml:mi>s</mml:mi></mml:math> Absorption Edge. Physical Review Letters. 2013. 110. 177401.	2.9	42
168	Soft x-ray scattering facility at the Advanced Light Source with real-time data processing and analysis. Review of Scientific Instruments, 2012, 83, 045110.	0.6	420
169	Elucidating Molecular Iridium Water Oxidation Catalysts Using Metal–Organic Frameworks: A Comprehensive Structural, Catalytic, Spectroscopic, and Kinetic Study. Journal of the American Chemical Society, 2012, 134, 19895-19908.	6.6	322
170	Tetrathiafulvalene Hetero Radical Cation Dimerization in a Redox-Active [2]Catenane. Journal of the American Chemical Society, 2012, 134, 19136-19145.	6.6	40
171	Electrochemical Water Oxidation with Carbon-Grafted Iridium Complexes. ACS Applied Materials & Interfaces, 2012, 4, 608-613.	4.0	69
172	Chiral metal–organic frameworks with tunable open channels as single-site asymmetric cyclopropanation catalysts. Chemical Communications, 2012, 48, 6508.	2.2	50
173	Mesoporous Block Copolymer Morphology Studied by Contrast-Matched Resonant Soft X-ray Scattering. Macromolecules, 2012, 45, 9188-9195.	2.2	25
174	Metal–Organic Frameworks for Light Harvesting and Photocatalysis. ACS Catalysis, 2012, 2, 2630-2640.	5.5	714
175	Cross-linked Polymers with Exceptionally High Ru(bipy) ₃ ²⁺ Loadings for Efficient Heterogeneous Photocatalysis. ACS Catalysis, 2012, 2, 417-424.	5.5	83
176	Light-Harvesting Cross-Linked Polymers for Efficient Heterogeneous Photocatalysis. ACS Applied Materials & Interfaces, 2012, 4, 2288-2294.	4.0	72
177	Oxygen sensing via phosphorescence quenching of doped metal–organic frameworks. Journal of Materials Chemistry, 2012, 22, 10329.	6.7	89
178	Chiral porous metal-organic frameworks with dual active sites for sequential asymmetric catalysis. Proceedings of the Royal Society A: Mathematical, Physical and Engineering Sciences, 2012, 468, 2035-2052.	1.0	35
179	Solventâ€dependent groundâ€state distributions in a donor–acceptor redoxâ€active bistable [2]catenane. Journal of Physical Organic Chemistry, 2012, 25, 544-552.	0.9	15
180	Cavity-induced enantioselectivity reversal in a chiral metal–organic framework BrÃ,nsted acid catalyst. Chemical Science, 2012, 3, 2623.	3.7	120

#	Article	IF	CITATIONS
181	Polarized X-ray scattering reveals non-crystalline orientational ordering in organic films. Nature Materials, 2012, 11, 536-543.	13.3	281
182	Rational Synthesis of Noncentrosymmetric Metal–Organic Frameworks for Second-Order Nonlinear Optics. Chemical Reviews, 2012, 112, 1084-1104.	23.0	921
183	The effects of conformation on the noncovalent bonding interactions in a bistable donor–acceptor [3]catenane. Chemical Communications, 2012, 48, 9245.	2.2	17
184	Pt Nanoparticles@Photoactive Metal–Organic Frameworks: Efficient Hydrogen Evolution via Synergistic Photoexcitation and Electron Injection. Journal of the American Chemical Society, 2012, 134, 7211-7214.	6.6	657
185	A Chiral Porous Metal–Organic Framework for Highly Sensitive and Enantioselective Fluorescence Sensing of Amino Alcohols. Journal of the American Chemical Society, 2012, 134, 9050-9053.	6.6	397
186	A rigid donor–acceptor daisy chain dimer. Chemical Communications, 2012, 48, 6791.	2.2	22
187	Metalâ€Organic Framework Templated Synthesis of Fe ₂ O ₃ /TiO ₂ Nanocomposite for Hydrogen Production. Advanced Materials, 2012, 24, 2014-2018.	11.1	407
188	Efficient Polymer Solar Cells Based on a Low Bandgap Semi rystalline DPP Polymerâ€₽CBM Blends. Advanced Materials, 2012, 24, 3947-3951.	11.1	209
189	Multiâ€Lengthâ€Scale Morphologies in PCPDTBT/PCBM Bulkâ€Heterojunction Solar Cells. Advanced Energy Materials, 2012, 2, 683-690.	10.2	171
190	Stimulated Release of Sizeâ€Selected Cargos in Succession from Mesoporous Silica Nanoparticles. Angewandte Chemie - International Edition, 2012, 51, 5460-5465.	7.2	157
191	Donor–Acceptor Ringâ€inâ€Ring Complexes. Chemistry - A European Journal, 2012, 18, 202-212.	1.7	40
192	A chiral metal–organic framework for sequential asymmetric catalysis. Chemical Communications, 2011, 47, 8256.	2.2	172
193	A neutral redox-switchable [2]rotaxane. Organic and Biomolecular Chemistry, 2011, 9, 7126.	1.5	26
194	Highly Stable and Porous Cross-Linked Polymers for Efficient Photocatalysis. Journal of the American Chemical Society, 2011, 133, 2056-2059.	6.6	394
195	Diffusion-Controlled Luminescence Quenching in Metalâ ^{~,} Organic Frameworks. Journal of the American Chemical Society, 2011, 133, 4232-4235.	6.6	199
196	Defining the Nanostructured Morphology of Triblock Copolymers Using Resonant Soft X-ray Scattering. Nano Letters, 2011, 11, 3906-3911.	4.5	139
197	Hierarchical Nanomorphologies Promote Exciton Dissociation in Polymer/Fullerene Bulk Heterojunction Solar Cells. Nano Letters, 2011, 11, 3707-3713.	4.5	415
198	Doping Metal–Organic Frameworks for Water Oxidation, Carbon Dioxide Reduction, and Organic Photocatalysis. Journal of the American Chemical Society, 2011, 133, 13445-13454.	6.6	1,363

#	Article	IF	CITATIONS
199	Actuation of Asymmetric Cyclopropanation Catalysts: Reversible Singleâ€Crystal to Singleâ€Crystal Reduction of Metal–Organic Frameworks. Angewandte Chemie - International Edition, 2011, 50, 8674-8678.	7.2	165
200	Interfaces in organic devices studied with resonant soft x-ray reflectivity. Journal of Applied Physics, 2011, 110, .	1.1	27
201	Isolation by crystallization of translational isomers of a bistable donor-acceptor [2]catenane. Proceedings of the National Academy of Sciences of the United States of America, 2010, 107, 13991-13996.	3.3	39
202	Isoreticular Chiral Metalâ ``Organic Frameworks for Asymmetric Alkene Epoxidation: Tuning Catalytic Activity by Controlling Framework Catenation and Varying Open Channel Sizes. Journal of the American Chemical Society, 2010, 132, 15390-15398.	6.6	635
203	Multistimuli Responsive Organogels Based on a New Gelator Featuring Tetrathiafulvalene and Azobenzene Groups: Reversible Tuning of the Gelâ^'Sol Transition by Redox Reactions and Light Irradiation. Journal of the American Chemical Society, 2010, 132, 3092-3096.	6.6	265
204	Nanomorphology of Bulk Heterojunction Photovoltaic Thin Films Probed with Resonant Soft X-ray Scattering. Nano Letters, 2010, 10, 2863-2869.	4.5	182
205	Synthesis, crystal structure, and magnetic properties of K4Mn3(HPO4)4(H2PO4)2. Solid State Sciences, 2009, 11, 845-851.	1.5	10
206	An Hg ²⁺ â€Gated Chiral Molecular Switch Created by Using Binaphthalene Molecules with Two Anthracene Units and Two 1,3â€Dithioleâ€2â€thione (1,3â€Dithioleâ€2â€one) Units. Chemistry - A Europea Journal, 2008, 14, 5680-5686.	an 1.7	24
207	Resonant soft x-ray reflectivity of organic thin films. Journal of Vacuum Science and Technology A: Vacuum, Surfaces and Films, 2007, 25, 575-586.	0.9	67
208	Chiral Molecular Switches Based on Binaphthalene Molecules with Anthracene Moieties:  CD Signal Due to Interchromophoric Exciton Coupling and Modulation of the CD Spectrum. Journal of Organic Chemistry, 2007, 72, 4306-4312.	1.7	21
209	New Organogels Based on an Anthracene Derivative with One Urea Group and Its Photodimer: Fluorescence Enhancement after Gelation. Langmuir, 2007, 23, 9195-9200.	1.6	98
210	A Chiral Low-Molecular-Weight Gelator Based on Binaphthalene with Two Urea Moieties:Â Modulation of the CD Spectrum after Gel Formation. Langmuir, 2007, 23, 1478-1482.	1.6	96
211	Thermal modulation of the monomer/excimer fluorescence for bispyrene molecules through the gel–solution transition of an organogel: A thermo-driven molecular fluorescence switch. Chemical Physics Letters, 2006, 428, 130-133.	1.2	26
212	Soft x-ray resonant reflectivity of low-Z material thin films. Applied Physics Letters, 2005, 87, 214109.	1.5	103
213	A Low-Molecular-Mass Gelator with an Electroactive Tetrathiafulvalene Group:Â Tuning the Gel Formation by Charge-Transfer Interaction and Oxidation. Journal of the American Chemical Society, 2005–127–16372-16373	6.6	251